Microfluidic Synthesis

Deutsche Ausgabe: DOI: 10.1002/ange.201600081
Internationale Ausgabe: DOI: 10.1002/anie.201600081

Microfluidic Synthesis Enables Dense and Uniform Loading of Surfactant-Free PtSn Nanocrystals on Carbon Supports for Enhanced Ethanol Oxidation

Fuxiang Wu[+], Dongtang Zhang[+], Manhua Peng, Zhihui Yu, Xiayan Wang, Guangsheng Guo, and Yugang Sun*

Abstract: *Developing new synthetic methods for carbon supported catalysts with improved performance is of fundamental importance in advancing proton exchange membrane fuel cell (PEMFC) technology. Continuous-flow, microfluidic reactions in capillary tube reactors are described, which are capable of synthesizing surfactant-free, ultrafine PtSn alloyed nanoparticles (NPs) on various carbon supports (for example, commercial carbon black particles, carbon nanotubes, and graphene sheets). The PtSn NPs are highly crystalline with sizes smaller than 2 nm, and they are highly dispersed on the carbon supports with high loadings up to 33 wt %. These characteristics make the as-synthesized carbon-supported PtSn NPs more efficient than state of the art commercial Pt/C catalysts applied to the ethanol oxidation reaction (EOR). Significantly enhanced mass catalytic activity (two-times that of Pt/C) and improved stability are obtained.*

Direct liquid ethanol fuel cells (DEFCs) are of interest because of their high power energy density, potential range of applications, low cost, and the convenient storage/delivery qualities of liquid fuels.[1–4] In a DEFC, catalysts for the ethanol oxidation reaction (EOR) essentially determine the performance and overall cost of the DEFC. State of the art electrocatalysts consist of carbon supported Pt (Pt/C) because metallic Pt is very active in C–C bond cleavage in the EOR.[5,6] However, the high cost and scarcity of Pt, as well as the facile poisoning of Pt surfaces upon formation of reaction intermediates, limits the practical applications of DEFCs containing Pt/C catalyst. Therefore, developing more efficient Pt-based bimetallic catalysts within which use of the precious metal Pt is reduced, with enhanced catalytic activity and improved stability, is a key research direction. For instance, Pt-based bimetallic alloy nanoparticles (NPs: PtRu, PtRh, PtSn, PtPd, and PtNi, among others) promote catalytic activity and alleviate catalyst poisoning.[7–10] Previous reports indicate that PtSn NPs exhibit catalytic activity greater than that of other reported Pt-based bimetallic NPs because of adsorption of OH species on Sn surfaces at low potentials, which can change the electronic structure of Pt atoms in PtSn to favor EOR.[4,5,11–15] Forming EOR catalysts usually requires multiple steps, including colloidal synthesis of PtSn NPs, loading of the synthesized PtSn colloidal NPs onto carbon supports,[16,17] and selective removal of surfactant layers on the PtSn NPs. Synthesis of monodisperse ultrafine PtSn NPs involves the use of surfactants, such as poly (vinylpyrrolidone) (PVP),[16] tetradecyltrimethylammonium bromide (TTAB),[17] and cetyltrimethylammonium bromide/chloride (CTAB/C),[18] which attach to the PtSn NP surfaces to prevent aggregation and shape distortion of NPs. The surfactant layers on the PtSn NPs usually block the access of reaction species to the catalytically active Pt atoms, significantly reducing their activity. Removing surfactant layers usually requires post-treatment in harsh environments (high-temperature annealing for example), which can cause severe sintering of ultrafine PtSn NPs. Therefore, simple methods are sought that can directly grow ultrafine and surfactant-free PtSn nanocrystals on carbon supports.[19–21]

Herein, we report the use of microfluidic reactions in a capillary tube reactor for rapid synthesis of ultrafine, surfactant-free PtSn alloy nanocrystals that are directly deposited on various carbon supports with high-density and uniform loading. The as-synthesized PtSn NPs exhibit an average size less than 2 nm, regardless of the type of carbon support used, and the loading of PtSn NPs can be as high as 33 wt % (Pt content is ca. 22 wt %). The as-synthesized carbon-supported PtSn NPs present significantly enhanced catalytic activity and stability towards EOR in comparison with the commercially available Pt/C catalyst.

Microfluidic reactions offer many advantages, including enhanced heat and mass transfer, rapid and tunable mixing of precursor solutions, continuous flow leading to reduced reaction time, and low reagent consumption throughout the course of optimization.[22–27] Such characteristics have encouraged researchers to explore the use of continuous flow-based microfluidic devices for synthesis of NPs with improved uniformity on a large scale.[28–34] Additionally, microfluidic reactors can be operated under hydrothermal and solvothermal conditions, and limited mass diffusion in a confined volume leads to reaction kinetics significantly different from that of conventional bulk solution reactions. Both attributes are expected to benefit the synthesis of uniform PtSn NPs on

[*] F. Wu,[+] D. Zhang,[+] M. Peng, Prof. Z. Yu, Prof. X. Wang, Prof. G. Guo
Beijing Key Laboratory for Green Catalysis and Separation, Department of Chemistry and Chemical Engineering, Beijing University of Technology
Beijing 100124 (P.R. China)
E-mail: xiayanwang@bjut.edu.cn
D. Zhang,[+] Prof. Y. Sun
Department of Chemistry, Temple University
Philadelphia, PA 19122 (USA)
[+] These authors contributed equally to this work.

Supporting information for this article can be found under http://dx.doi.org/10.1002/anie.201600081.

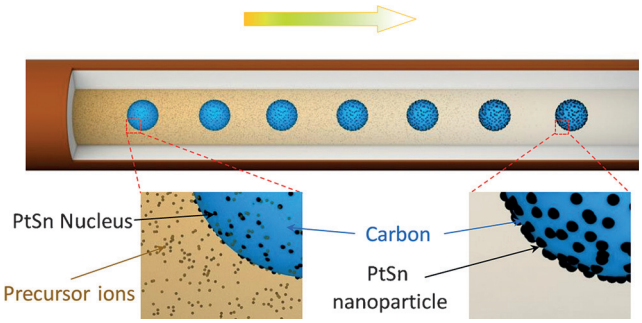

Figure 1. Formation of ultrafine PtSn NPs on a carbon sphere with uniform loading in a microfluidic reactor with a confined lateral dimension.

carbon supports, such as carbon black particles of XC-72. Figure 1 displays the capillary microfluidic system used to directly grow ultrafine PtSn NPs on carbon spheres. The reaction solution containing carbon black particles and precursor metal ions is pressurized in a chamber using pressure-regulated nitrogen gas to flow reaction mixture into the capillary tube reactor. The applied pressure makes it possible to realize reactions at temperatures higher than the boiling point of the reaction solvent. Once the reaction solution flows to the heating region, where the capillary tube is maintained at an elevated temperature, the reaction solution in the tube can be quickly heated to the desired temperature within a very short time[35] because of the rapid heat transfer in the thin capillary tube wall and the small volume of solution in the capillary tube. The fast increase of reaction temperature to a constant value leads to a high reduction rate of H_2PtCl_6 and $SnCl_4$ precursors, achieving supersaturated concentrations of metal atoms in a very short reaction time. The supersaturated Pt and Sn atoms nucleate on the surface of the carbon spheres in a well-dispersed fashion because heterogeneous nucleation is kinetically preferable compared to homogeneous nucleation. Following reduction of precursors, selective growth of existing PtSn NPs occurs rather than formation of new NPs. In the pressurized flow microfluidic reactor, diffusion of precursor species along the flow direction (that is, the longitudinal direction of the capillary tube) is suppressed. The small diameter of the capillary tube reactor limits the availability of precursors responsible for growth of PtSn NPs, ensuring that the PtSn NPs on carbon spheres are small in size. Interactions between NPs and carbon support consist of covalent bonds between PtSn atoms and carboxyl groups on the support. Carbon supports were activated by soaking in an aqueous solution of HNO_3, leading to formation of carboxyl groups by oxidation of surface carbon atoms. Surface carboxyl groups provide nucleation sites for formation of PtSn nanocrystals because of strong coordinative interactions between PtSn atoms and carboxyl groups.[36] Within roughly 10 s, the reaction solution is able to flow through the capillary tube reactor (with a length of 1.3 m, including a heating region of 1.2 m and a cooling region of 0.1 m) to the outlet, where the products are collected. When the reaction solution flows from the heating region to the cooling region, a drop in temperature leads to quick cessation of precursor reduction, as well as possible sintering of PtSn NPs. Since the carbon black spheres are well-dispersed in ethylene glycol, the corresponding carbon spheres loaded with PtSn NPs are also well-dispersed. Good colloidal dispersity is also beneficial for preventing the capillary tube reactor from becoming blocked, enabling continuous synthesis with high efficiency.

Figure 2 presents transmission electron microscopy (TEM) images of the product formed in the capillary tube reactor from the simultaneous reduction of H_2PtCl_6 and $SnCl_4$

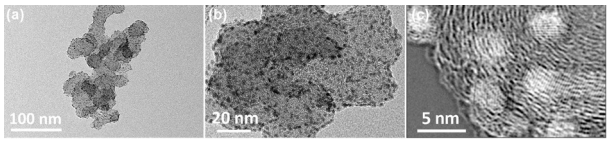

Figure 2. Variously magnified TEM images of PtSn NPs grown on XC-72 carbon particles.

in the presence of carbon black spheres (XC-72). An X-ray diffraction (XRD) pattern of the product indicates that the metal NPs (tiny dark dots in Figure 2) are a PtSn alloy with a face-centered cubic lattice and a lattice constant larger than metallic Pt (Supporting Information, Figures S1 and S2). All PtSn NPs are deposited on the carbon spheres and free-standing PtSn NPs are essentially absent (Figure 2a), confirming that heterogeneous nucleation of PtSn on the carbon spheres is favored. By contrast, in the absence of carbon spheres homogeneous nucleation is favored, forming free-standing PtSn NPs (Supporting Information, Figure S4). The dispersity of PtSn NPs on the surface of carbon spheres is fairly uniform, increasing surface exposure of PtSn NPs by ensuring sufficient separation of particles, which is beneficial for catalysis. The high-resolution TEM (HRTEM) image in Figure 2c and Figure S5A (Supporting Information) clearly highlight the lattice fringes of the PtSn nanocrystals and the gaps between adjacent crystalline domains, confirming the exposure of crystalline PtSn surfaces. Statistical analysis of 100 PtSn NPs reveals a narrow size distribution with an average of 1.86 nm (Supporting Information, Figure S3). Given that surfactant is absent from the synthesis, PtSn NPs on the XC-72 carbon spheres (PtSn/XC-72) expose clean surfaces.

This microfluidic reaction is also capable of directly growing surfactant-free PtSn naoncrystals on other carbon supports, such as one-dimensional (1D) carbon nanotubes (CNTs) and two-dimensional (2D) graphene sheets formed by reduction of exfoliated graphene oxide (rGO). Figure 3 presents TEM images of the as-synthesized composites, consisting of PtSn NPs on CNTs (PtSn/CNT, Figure 3a–c; Supporting Information, Figure S5B) and PtSn nanocrystals on rGO (PtSn/rGO, Figure 3d–f; Supporting Information, Figure S5C), clearly showing the uniform and dense dispersity of PtSn NPs on the surfaces of the carbon supports. The average sizes of the PtSn NPs are 1.98 nm and 1.85 nm for PtSn/CNT and PtSn/rGO samples, respectively. Much like PtSn NPs on XC-72 carbon spheres, PtSn NPs (Figure 3) exhibit face-centered cubic lattices with lattice constants

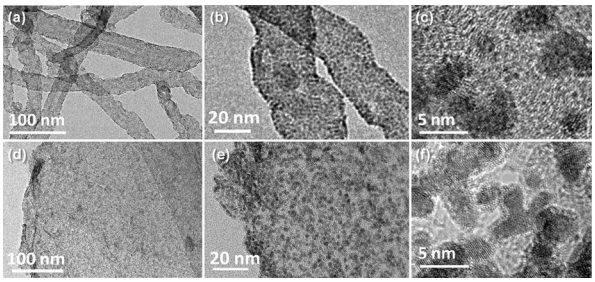

Figure 3. TEM and HRTEM images of the PtSn NPs grown on (a–c) multiple-walled carbon nanotubes (MWCNTs) and (d–f) reduced graphene sheets. Circular lattice fringes with larger spacing in (c) correspond to a MWCNT.

larger than that of Pt nanocrystals in commercial Pt/C (Supporting Information, Figure S1). However, the lattice constants and crystalline interplanar distances (d) of PtSn nanocrystals are slightly different in samples with different carbon supports (Supporting Information, Figure S2 and Table S1), indicating that the type of carbon support has a slight influence on the compositional ratio of Sn/Pt in the PtSn nanocrystals. The ratio of XRD peak areas in the synthesized samples is essentially the same as that of Pt in a commercial Pt/C sample, implying that the type of carbon support does not influence the morphological isotropy of the PtSn nanocrystals (Supporting Information, Table S1).

The EOR catalytic activity of the as-synthesized PtSn/XC-72, PtSn/CNT, and PtSn/rGO materials was investigated electrochemically, by modifying a glassy carbon electrode with the aforementioned composites. Figure 4A shows the cyclic voltammetry (CV) curves of the modified electrodes in

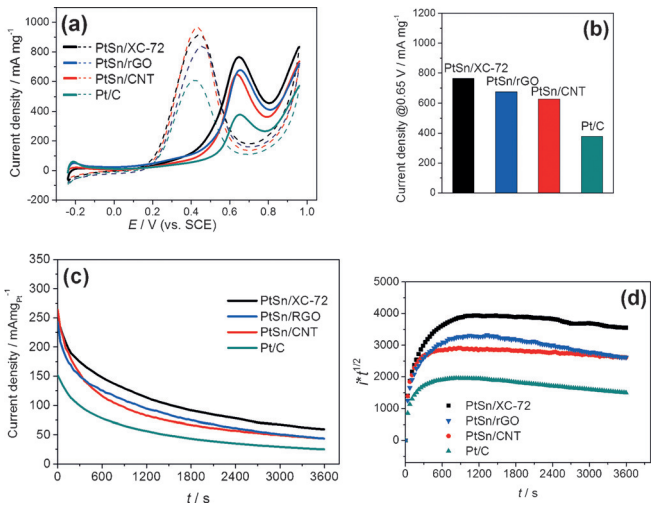

Figure 4. a) CV curves recorded from electrodes coated with synthesized PtSn/XC-72 (Figure 2), PtSn/rGO (Figure 3d–f), PtSn/CNT (Figure 3a–c), and commercial Pt/C in an aqueous solution of H_2SO_4 (0.5 M) and C_2H_5OH (1 M) at room temperature. Scan rate (50 mV s^{-1}), current densities normalized against the mass of metallic Pt loaded onto the electrodes. b) Comparison of the current density (i) over time (t) at 0.65 V (vs. SCE) for electrodes modified with different catalysts. c) Chronoamperometric curves measured at 0.45 V (vs. SCE) for electrodes modified with different catalysts. d) Calculated $it^{1/2}$ as a function of time.

an aqueous solution of H_2SO_4 (0.5 M) and C_2H_5OH (1 M) at room temperature. The current density of each CV curve is normalized against the Pt loading on the electrode, showing a significant difference in catalytic activity of the different catalysts. In each CV curve, an obvious anodic peak corresponding to EOR is observed as potential is scanned from −0.24 V to 0.96 V (vs. SCE). The scanning potential in the reverse direction reveals a cathodic peak corresponding to the reduction of species formed by ethanol oxidation. It is clear that the EOR current density of electrodes modified with synthesized PtSn nanocrystals is always higher than that on the electrode modified with the commercial Pt/C catalyst (see the forward CV peaks, solid curves). For example, the mass activities of different catalysts at 0.65 V are 764.1 mA mg^{-1}, 675.4 mA mg^{-1}, 628.8 mA mg^{-1}, and 377.8 mA mg^{-1}; respectively corresponding to PtSn/XC-72, PtSn/rGO, PtSn/CNT, and Pt/C catalysts (Figure 4b). The EOR results indicate that the synthesized PtSn/XC-72, PtSn/rGO, and PtSn/CNT catalysts respectively achieve 2.02, 1.78, and 1.66 times the mass activity of state of the art commercial Pt/C catalyst. The higher activity of PtSn/XC-72 and PtSn/rGO compared to PtSn/CNT may be a result of the smaller size of PtSn nanocrystals on XC-72 and rGO supports (1.86 nm on XC-72 and 1.85 nm on rGO, versus 1.98 nm on CNT). Smaller nanocrystal sizes provide higher surface areas for reacting species to access. Additionally, the onset potentials for EOR on PtSn/XC-72, PtSn/rGO, and PtSn/CNT, are 9.9, 3.0, and 4.8 mV, respectively, which are lower than that measured on commercial Pt/C (43.6 mV). Lower onset potentials indicate that fuel cells using the synthesized PtSn catalysts offer higher output voltages. Collectively, enhanced current density and lowered onset potential indicate that PtSn NPs supported on various carbon supports synthesized by microfluidic reactions are new and efficient catalysts for EOR. Figure 4c presents chronoamperometric curves at 0.45 V measured in H_2SO_4 (0.5 M) and ethanol (1 M) for electrodes modified with different catalysts. Once again, a comparison of the aforementioned materials shows that PtSn/XC-72, PtSn/rGO, and PtSn/CNT achieve higher catalytic current densities than commercial Pt/C. Under chronoamperometric conditions, the current density is determined by mass diffusion after a long period, at which point limiting diffusion conditions are established. According to the Cottrell equation $i(t) = i_d(t) = \frac{nFAD_0^{1/2}C_0^*}{\pi^{1/2}t^{1/2}}$, $i(t)t^{1/2}$ is equal to $\frac{nFAD_0^{1/2}C_0^*}{\pi^{1/2}}$, which represents a constant value at a specific temperature because the electron transfer number (n), Faraday constant (F), electrode surface area (A), and concentration of ethanol in the bulk solution (C_0^*) are all constants. If the activity of a catalyst decreases, the electrochemically active electrode surface area may be lowered; possibly because the PtSn NPs fall off the electrode, or the catalytically active surfaces of the PtSn NPs are poisoned during reaction. Both factors can lower the value of $\frac{nFAD_0^{1/2}C_0^*}{\pi^{1/2}}$. As shown in Figure 4d, $it^{1/2}$ reaches a maximum followed by a gradual decrease over longer time periods. The slow drop of $it^{1/2}$ corresponds to a decrease in activity and stability of the catalysts. In the case of PtSn/XC-72 and PtSn/CNT, $it^{1/2}$ decreases more slowly than it does for Pt/C, indicating that the synthesized PtSn NPs on XC-72

and CNT are more stable than the Pt NPs of the commercial Pt/C catalyst in an aqueous acidic ethanol solution. In contrast, the $it^{1/2}$ value of PtSn/rGO drops faster than that of Pt/C; probably because of oxidation of rGO, which reduces the electrical conductivity of the rGO support in turn. The comparison shown in Figure 4d clearly indicates that the as-synthesized PtSn/C catalysts exhibit higher stability than the commercial Pt/C catalyst. Although pure Sn metal is more susceptible to corrosion in an acidic environment than pure Pt metal, Sn atoms in the PtSn alloy lattice impart resistance as a result of coordinative interactions with Pt atoms in the PtSn alloy lattice.[4]

In summary, surfactant-free PtSn NPs on various carbon supports, particularly on commercial carbon black particles of XC-72, exhibit much higher EOR catalytic activity and significantly improved stability compared to state of the art commercial Pt/C catalyst. These improvements showcase the advantages of microfluidic reactions performed in capillary tube reactors, which enable the growth of PtSn alloy NPs directly on various carbon supports with high dispersity and uniformity. The absence of surfactant in the described reactions allows formation of intimate contact between the PtSn nanocrystals and carbon supports, which facilitates charge transfer in catalytic EOR. Furthermore, clean PtSn surfaces are exposed, which provide a high-density of catalytically active sites. In contrast with 3D diffusion of precursors in conventional reactors, quasi 2D diffusion of precursors is favored by capillary tube reactors, limiting the availability of precursors to growth of individual PtSn nanocrystals and consequently allowing formation of PtSn nanocrystals of small sizes. Moreover, precise control over temperature in different zones of a capillary tube reactor, coupled with continuous flow synthesis, suggest that the techniques described herein offer improved control in large scale processes. Our results demonstrate the significant promise of microfluidic reactions in synthesis of important catalysts on desirable supports.

Experimental Section

Synthesis of PtSn NPs on carbon supports: syntheses were performed using a microfluidic reactor system (involving the use of capillary tubes), reported in our previous work.[25] A typical synthesis of PtSn NPs loaded on carbon black particles (Vulcan XC-72, Cabot Corporation) involved addition of $SnCl_4{\cdot}5H_2O$ (0.1 mmol) and $H_2PtCl_6{\cdot}6H_2O$ (0.1 mmol) to ethylene glycol (100 mL) in a flask. An appropriate amount of XC-72 (40 mg) was then added to the solution, followed by ultrasonication for 5 min at room temperature. The reaction solution, containing carbon black particles and precursor metal ions, was pressurized in a chamber using pressure-regulated nitrogen gas to flow reaction mixture into the capillary tube reactor. Reduction of metal ions occurred in the heating region of the microscale capillary tube (120 cm). Cessation of growth of PtSn NPs occurred in the cooling region (10 cm). The products were collected by an aspiration filtration process, and subsequently washed with ethanol and water three times. The collected precipitates were dried in an oven at 60 °C for 10 hours, resulting in the supported PtSn catalysts, which were characterized. Carbon materials, such as reduced graphene oxide (rGO) purchased from Graphene Supermarket, and multiple-walled carbon nanotubes (CNTs) purchased from Chengdu Organic Chemicals Co. Ltd., were used as supports for PtSn NPs. Further experimental and characterization details (for example, XRD, refined XRD, TEM, and electrochemical characterization) are described in the Supporting Information.

Acknowledgements

This work was financially supported by the National Natural Science Foundation of China (No. 21275014, 21375005), and the Program for New Century Excellent Talents in University (NCET-12-0603), the Importation and Development of High-Caliber Talents Project of Beijing Municipal Institutions (CIT&TCD20140309), and Beijing Natural Science Foundation Program and Scientific Research Key Program of Beijing Municipal Commission of Education (No. KZ201310005001). We thank Dr. Lin Gu and Mr. Yue Gong from the Institute of Physics Chinese Academy of Sciences for help with HRTEM experiments. Y.S. is thankful for start-up support from Temple University.

Keywords: carbon supports · electrocatalysis · ethanol oxidation reactions · microfluidic synthesis · platinum tin alloyed nanoparticles

How to cite: *Angew. Chem. Int. Ed.* **2016**, *55*, 4952–4956
Angew. Chem. **2016**, *128*, 5036–5040

[1] K. Artyushkova, B. Halevi, M. Padilla, P. Atanassov, E. A. Baranova, *J. Electrochem. Soc.* **2015**, *162*, H345–H351.
[2] J. Asgardi, J. C. Calderón, F. Alcaide, A. Querejeta, L. Calvillo, M. J. Lazaro, G. Garcia, E. Pastor, *Appl. Catal. B* **2015**, *168*, 33–41.
[3] D.-H. Kwak, Y.-W. Lee, S.-B. Han, E.-T. Hwang, H.-C. Park, M.-C. Kim, K.-W. Park, *J. Power Sources* **2015**, *275*, 557–562.
[4] S. C. Zignani, V. Baglio, E. R. Gonzalez, A. S. Aricò, *ChemElectroChem* **2014**, *1*, 1403–1406.
[5] S. Song, P. Tsiakaras, *Appl. Catal. B* **2006**, *63*, 187–193.
[6] E. Antolini, *J. Power Sources* **2007**, *170*, 1–12.
[7] S. B. Adler, *Chem. Rev.* **2004**, *104*, 4791–4844.
[8] V. R. Stamenkovic, B. S. Mun, M. Arenz, K. J. J. Mayrhofer, C. A. Lucas, G. Wang, P. N. Ross, N. M. Markovic, *Nat. Mater.* **2007**, *6*, 241–247.
[9] L. Liu, G. Samjeske, S.-i. Nagamatsu, O. Sekizawa, K. Nagasawa, S. Takao, Y. Imaizumi, T. Yamamoto, T. Uruga, Y. Iwasawa, *J. Phys. Chem. C* **2012**, *116*, 23453–23464.
[10] X. Li, L. An, X. Wang, F. Li, R. Zou, D. Xia, *J. Mater. Chem.* **2012**, *22*, 6047–6052.
[11] Y. Ma, H. Wang, S. Ji, V. Linkov, R. Wang, *J. Power Sources* **2014**, *247*, 142–150.
[12] E. Antolini, E. R. Gonzalez, *Catal. Today* **2011**, *160*, 28–38.
[13] R. B. Kutz, B. Braunschweig, P. Mukherjee, R. L. Behrens, D. D. Dlott, A. Wieckowski, *J. Catal.* **2011**, *278*, 181–188.
[14] V. Alzate, K. Fatih, H. Wang, *J. Power Sources* **2011**, *196*, 10625–10631.
[15] W. J. Zhou, S. Q. Song, W. Z. Li, Z. H. Zhou, G. Q. Sun, Q. Xin, S. Douvartzides, P. Tsiakaras, *J. Power Sources* **2005**, *140*, 50–58.
[16] Y. Gao, X. Chen, J. Zhang, H. Asakura, T. Tanaka, K. Teramura, D. Ma, N. Yan, *Adv. Mater.* **2015**, *27*, 4688–4694.
[17] C. Zhang, S. Y. Hwang, A. Trout, Z. Peng, *J. Am. Chem. Soc.* **2014**, *136*, 7805–7808.
[18] Y. Sun, Y. Xia, *Science* **2002**, *298*, 2176–2179.
[19] K. M. Bratlie, H. Lee, K. Komvopoulos, P. Yang, G. A. Somorjai, *Nano Lett.* **2007**, *7*, 3097–3101.

[20] B. Nikoobakht, M. A. El-Sayed, *Chem. Mater.* **2003**, *15*, 1957 – 1962.
[21] Y. Tang, F. Gao, S. Yu, Z. Li, Y. Zhao, *J. Power Sources* **2013**, *239*, 374 – 381.
[22] S. Wang, L. Kuai, Y. Huang, X. Yu, Y. Liu, W. Li, L. Chen, B. Geng, *Chem. Eur. J.* **2013**, *19*, 240 – 248.
[23] Z. Sun, J. Masa, W. Xia, D. Koenig, A. Ludwig, Z.-A. Li, M. Farle, W. Schuhmann, M. Muhler, *ACS Catal.* **2012**, *2*, 1647 – 1653.
[24] L. Zhang, Y. Wang, L. Tong, Y. Xia, *Nano Lett.* **2014**, *14*, 4189 – 4194.
[25] L. Zhang, G. Niu, N. Lu, J. Wang, L. Tong, L. Wang, M. J. Kim, Y. Xia, *Nano Lett.* **2014**, *14*, 6626 – 6631.
[26] G. Niu, A. Ruditskiy, M. Vara, Y. Xia, *Chem. Soc. Rev.* **2015**, *44*, 5806 – 5820.
[27] P. W. Dunne, A. S. Munn, C. L. Starkey, T. A. Huddle, E. H. Lester, *Philos. Trans. R. Soc. London Ser. A* **2015**, DOI: 10.1098/rsta.2015.0015.
[28] M.-S. Rhee, P. M. Valencia, M. I. Rodriguez, R. Langer, O. C. Farokhzad, R. Karnik, *Adv. Mater.* **2011**, *23*, H79 – H83.
[29] P. M. Valencia, O. C. Farokhzad, R. Karnik, R. Langer, *Nat. Nanotechnol.* **2012**, *7*, 623 – 629.
[30] S. Marre, K. F. Jensen, *Chem. Soc. Rev.* **2010**, *39*, 1183 – 1202.
[31] D. Zhang, F. Wu, M. Peng, X. Wang, D. Xia, G. Guo, *J. Am. Chem. Soc.* **2015**, *137*, 6263 – 6269.
[32] L. Zhang, Y. Xia, *Adv. Mater.* **2014**, *26*, 2600 – 2606.
[33] A. Abou-Hassan, O. Sandre, V. Cabuil, *Angew. Chem. Int. Ed.* **2010**, *49*, 6268 – 6286; *Angew. Chem.* **2010**, *122*, 6408 – 6428.
[34] Y. Song, J. Hormes, C. S. S. R. Kumar, *Small* **2008**, *4*, 698 – 711.
[35] J. Puigmartí-Luis, *Chem. Soc. Rev.* **2014**, *43*, 2253 – 2271.
[36] K. Kordas, A.-R. Rautio, G. S. Lorite, M. Mohl, P. Mäki-Arvela, J.-P. Mikkola, D. Murzin, L. Ge, P. M. Ajayan, R. Vajtai, *Top. Catal.* **2015**, *58*, 1127 – 1135.

Received: January 4, 2016
Revised: February 10, 2016
Published online: March 15, 2016

